



Effect of infiltration on the performance of an unsaturated geotextile-reinforced soil wall



F.H.M. Portelinha ^{a,*}, J.G. Zornberg ^b

^a Federal University of Sao Carlos, Civil Engineering Department - DECiv, Washington Luis Roadway, km 235, mailbox 676, Sao Carlos, Sao Paulo, 13.565-905, Brazil

^b The University of Texas at Austin, Civil Engineering Department – GEO, 1 University Station C1792, Austin, TX 78712-0280, USA

ARTICLE INFO

Article history:

Received 1 April 2016

Received in revised form

12 January 2017

Accepted 10 February 2017

Available online 23 February 2017

Keywords:

Geosynthetics

Infiltration

Reinforced soil wall

Capillary break

Suction

ABSTRACT

A full-scale geotextile-reinforced soil wall was built in order to assess the characteristics of water infiltration and its effect on the structure performance. Nonwoven geotextiles were selected as inclusions in order to provide not only reinforcement, but also internal drainage to the fine-grained soil used as backfill material. The structure was built in a laboratory setting, which facilitated implementation of a thorough instrumentation plan to measure volumetric water content changes of soil, suction, facing displacements and reinforcement strains. An irrigation system was used to simulate controlled rainfall events. The monitoring program allowed the evaluation of the advancement of infiltration and internal geosynthetic drainage. Evaluation of the effect of the hydraulic response on the overall performance of the structure included assessment of the development of capillary breaks at soil-geotextiles interfaces. Capillary breaks resulted in water storage above the geotextile reinforcements and led to retardation of the infiltration front in comparison to the infiltration that would occur without the presence of permeable reinforcements. After breakthrough, water was also found to migrate along the geotextiles, suggesting that the reinforcement layers ultimately provided in-plane drainage capacity. While generation of positive pore water pressures was not evidenced during the tests, the advancing infiltration front was found to affect the performance of the wall. Specifically, infiltration led to increasing reinforcement strains and facing displacements, as well as to the progressive loss of suction. While the accumulation of water due to the temporary capillary break also resulted in an increased backfill unit weight, its effect on deformation of the wall was not possible to be captured but it is intrinsic on the overall behavior observed in this study. Correlations between reinforcement strains/face displacement and the average of suction in the backfill soil, as measured by tensiometers in different locations within the backfill mass, point to the relevance of the suction as a representative indicator of the deformability of the geotextile-reinforced wall subjected to water infiltration. Reinforcement strains and face displacements were found to reduce more significantly with reduction of suction until a certain value of suction from which the rate of decreasing declines.

© 2017 Elsevier Ltd. All rights reserved.

1. Introduction

Nonwoven geotextiles have often been reported to successfully reinforce fine-grained soils in earth retaining walls and embankments (Tatsuoka and Yamauchi, 1986; Gourc and Matichard, 1992; Mitchell and Zornberg, 1995; Wayne et al., 1996; Ehrlich et al., 1997; Benjamin et al., 2007; Portelinha et al., 2013, 2014). In particular,

the use of nonwoven geotextiles has been reported to facilitate the use of on-site fine-grained backfill materials, resulting in important cost savings. This is because the use of nonwoven geotextiles as reinforcement layers is expected to allow internal drainage that, in turn, leads to improved stability by dissipating pore water pressures during construction or precipitation events.

In fact, a number of the reported studies have indicated an adequate performance of geotextile-structures constructed using poorly draining backfill, even when subjected to significant periods of rainfall events (Carvalho et al., 1986; Tatsuoka and Yamauchi, 1986; Mitchell and Zornberg, 1995; Wayne et al., 1996; Portelinha

* Corresponding author.

E-mail addresses: fportelinha@ufscar.br (F.H.M. Portelinha), zornberg@mail.texas.edu (J.G. Zornberg).

et al., 2013, 2014).

The effectiveness of in-plane drainage provided by permeable geosynthetic reinforcements (e.g., nonwoven geotextiles, geocomposites) has been previously evaluated and quantified using different approaches (e.g. pullout tests, full-scale models, small-scale models). The benefits of minimizing the generation of positive pore water pressures has been a common finding in these studies (Perrier et al., 1986; Ling et al., 1993; Mitchell and Zornberg, 1995; Kempton et al., 2000; Tan et al., 2001; Zornberg and Kang, 2005; Ghionna et al., 2010; Portelinha et al., 2013; Bhattacharjee and Viswanadham, 2015; Thuo et al., 2015). Some of these studies have concluded that internal drainage enhances internal stability by facilitating the development of conditions corresponding to a drained soil behavior (Yamanouchi et al., 1982; Tatsuoka and Yamauchi, 1986; Yunoki and Nagao, 1988; Zornberg and Mitchell, 1994; Bhattacharjee and Viswanadham, 2015).

Since the water pressures within an unsaturated soil mass are negative, their understanding requires evaluation of the unsaturated hydraulic and mechanical characteristics of geosynthetics, backfill, and interfaces (Iryo and Rowe, 2005; Bouazza et al., 2013; Thuo et al., 2015; Vahedifard et al., 2016). Zornberg et al. (2010) reports the development of capillary breaks when nonwoven geotextiles underlay unsaturated soils. This is because under unsaturated conditions the hydraulic conductivity of nonwoven geotextiles is typically lower than that of the overlying soil. This phenomenon results in additional storage of moisture at the soil-geosynthetic interface until the suction decreases below a value identified as the “breakthrough” suction. The capillary break effect has been observed to increase the water storage capacity of soils (Stormont et al., 1997; Khire et al., 2000; McCartney and Zornberg, 2010).

Iryo and Rowe (2005) conducted finite element simulations of the hydraulic behavior of permeable geosynthetics within unsaturated embankments subjected to infiltration. The study showed that nonwoven geotextiles would delay water infiltration in situations where the soil pore water pressures are negative, whereas they would enhance drainage in situations where the pore water pressures are positive. The authors also found that nonwoven geotextiles would only act as internal drains after a moisture threshold has been reached and that drainage could be improved by installing the reinforcement on an inclined grade. This study also reported that the contribution of nonwoven geotextiles to the stability of embankments constructed with fine-grained soils is less relevant as a drainage material than as a reinforcement material. In a similar finite element study, Bhattacharjee and Viswanadham (2015) reported that the use of a hybrid-geosynthetic layers (i.e., dual function material providing drainage and reinforcement) is effective for reduction in excess pore water pressure. Further, the global stability of a hybrid-geosynthetic-reinforced slope was found to increase considerably, while the deformation values were significantly lower for the reinforced slope as compared with that of the unreinforced slope.

Garcia et al. (2007) tested small-scale reinforced embankment models built using permeable geosynthetics (nonwoven geotextiles, woven/nonwoven geocomposites and strips of nonwoven geotextiles). The embankments were subjected to cycles of wetting and drying. Pore water pressures (negative and positive) and volumetric water content values were monitored. The results showed that geosynthetics embedded within the soil showed drainage capabilities only when the pore water pressures of the overlying soil reached values close to zero or became positive. Local failure during the wetting process was reported when positive pore water pressures were observed to develop above the soil-geosynthetic interface. In models where strips of nonwoven geotextiles were used, water did not accumulate over the soil-

geotextile interface. Strips of geotextile were reported to prevent the development of capillary break and to allow drainage of water within the embankment.

Krisdani et al. (2010) built a small-scale slope model to simulate a sloping capillary break. The model involved a 0.20 m thick fine sand layer (as the fine-grained layer) and a nonwoven geotextile (as the coarse-grained layer). The objective was to investigate the development of capillary breaks and the efficiency of internal drainage layers. Rainfall events of different intensities and durations were applied over the model. The test results indicated that presence of the geosynthetic led to the development of a capillary break and prevented water infiltration into the underlying soil layer. Lateral diversion flow was found to develop along the fine-grained layer (fine sand), which was interpreted as an indication of the development of a capillary break during rainfall events.

Other relevant aspect to be assessed in unsaturated reinforced soil structures is the fact that suction might change when subject to infiltration resulting in reduction on shear strength and shear modulus of soil. In the last decades, many studies have been dedicated to describe the effect of suction on the shear strength of soils (Bishop et al., 1960; Fredlund and Morgenstern, 1977; Fredlund et al., 1978; Karube, 1988; Toll, 1990; Wheeler and Sivakumar, 1992; Vanapalli et al., 1996; Khalali and Khabazz, 1998). Recently, studies have been conducted in order to describe the relationship between suction and shear modulus of soil (Cabarkapa et al., 1999; Mancuso et al., 2002; Ng and Yung, 2008; Ng and Xu, 2012). Generally, authors have reported that the shear modulus increases until a certain value of suction from which no significant increases in modulus is reached. The rate of increasing declines when the suction is higher than the air-entry value of the soil.

In summary, while previous studies on the infiltration into unsaturated geotextile-reinforced soil systems have used small-scale models or numerical simulations, no full-scale study has been reported so far on this relevant issue. In particular, only limited information is currently available on the effect of water infiltration on the overall performance of geosynthetic-reinforced walls. This includes the lack of the quantification of wall deformations that could be induced by wetting and development of capillary breaks during infiltration. Accordingly, an important objective of this study is to evaluate the infiltration process into the unsaturated fill in a geotextile-reinforced wall and its effect on the structure mechanical response. This is achieved by monitoring the performance of a large-scale reinforced soil wall. The experimental program focuses specifically on the impact of infiltration into the backfill of a wall reinforced with nonwoven geotextiles. Reinforcement strains and face displacements are used as key aspects to quantify the wall performance.

2. Experimental program

The experimental program in this study involved monitoring the hydraulic and mechanical responses of a full-scale geotextile-reinforced wall subjected to infiltration. The model reported in this paper is part of a series of full-scale walls constructed in the Geosynthetics Laboratory of the Sao Carlos School of Engineering at the University of Sao Paulo, Brazil. The characteristics of the wall reported in this paper are discussed next.

2.1. Reinforced steel frame

A reinforced steel frame was used to house the series of full-scale reinforced soil wall structures, which were 1.8 m high and 1.55 m wide, with backfill soil extending to a distance of 1.8 m from the front edge of the box. The structure was founded on a rigid

concrete foundation. The soil was laterally confined by two parallel metallic counterfort walls bolted to a structural floor. The box includes a metallic lid that was bolted to the lateral walls in order to provide reaction during application of vertical loads. Specifically, the lid provided confinement to an air bag used to apply a uniform surcharge over the soil surface (up to 200 kPa). The back of the reinforced fill was also restrained by a metallic counterfort wall. The inside surfaces of the metallic box were lubricated with Vaseline® and covered with polyethylene sheeting in order to minimize side friction and to facilitate the development of plane-strain conditions. Lateral stresses and restrictions might have occurred during tests, but are negligible and not invalidate trends and parameters relations obtained in the experimental program.

2.2. Materials

A fine-grained soil was used to construct the full-scale geotextile-reinforced wall. Specifically, the soil is a clayey sand with a saturated hydraulic conductivity of 4.9×10^{-7} m/s. Physical characteristics of the soil are shown in Table 1. The soil particle size distribution (ASTM D422-63) indicates that the soil includes approximately 44% of fines. Accordingly, this backfill would not meet the AASHTO (2002) specifications for reinforced soil walls. The shear strength of the soil, evaluated using consolidated drained (CD) triaxial compression tests (ASTM D7181), resulted in a friction angle of 35° and zero cohesion. The soil water retention curve of the soil was obtained using the filter paper technique (ASTM D5298) and hanging column tests (ASTM D6836), considering both drying and wetting processes. The soil water retention curves are shown in Fig. 1a. The shape of curves was found to present a bimodal trend, which has been in the focus of several recent studies (Durner, 1994; Coppola, 2000; Peters and Durner, 2008; Schelle et al., 2010; Chamindu Deepagoda et al., 2012). The heterogeneous pore size distribution of the type of soil used in this study were observed to be similar to many others found in literature of which bimodal behavior of water retention curves were also reported. The bimodal curve was fitted in the experimental data by the use of Durner's model (Durner, 1994) applied to both drying and wetting process. The Durner's model is described as:

$$S_e = w_1 \left[\frac{1}{1 + (\alpha_1 \psi)^{n_1}} \right]^{m_1} + (1 - w_2) \left[\frac{1}{1 + (\alpha_2 \psi)^{n_2}} \right]^{m_2} \quad (1)$$

$$\theta = \theta_r + (\theta_s - \theta_r) S_e \quad (2)$$

where w_1 e w_2 are initial gravimetric water contents of each segment of the bimodal curve, ψ is the suction, S is the degree of saturation, θ_r is the residual volumetric water content and θ_s is the saturation volumetric water content. The parameters n_1, m_1, α_1 are fitting parameters of the first segment of the curve, while n_2, m_2, α_2

Table 1
Characteristics of the backfill soil.

Characteristics	Standard	Values
Clay fraction	ASTM D422-63	32%
Silt fraction		12%
Sand fraction		56%
G_s	ASTM D7263-09	2.75
Liquid limit	ASTM D4318-10e1	40%
Plastic limit	ASTM D4318-10e1	19%
Maximum dry unit weight	ASTM D1557	17.9 kN/m ³
Optimum water content	ASTM D1557	14.6%
Cohesion	ASTM D7181	0 kPa
Friction angle	ASTM D7181	35°
Saturated hydraulic conductivity	ASTM D5856-15	4.9×10^{-7} m/s

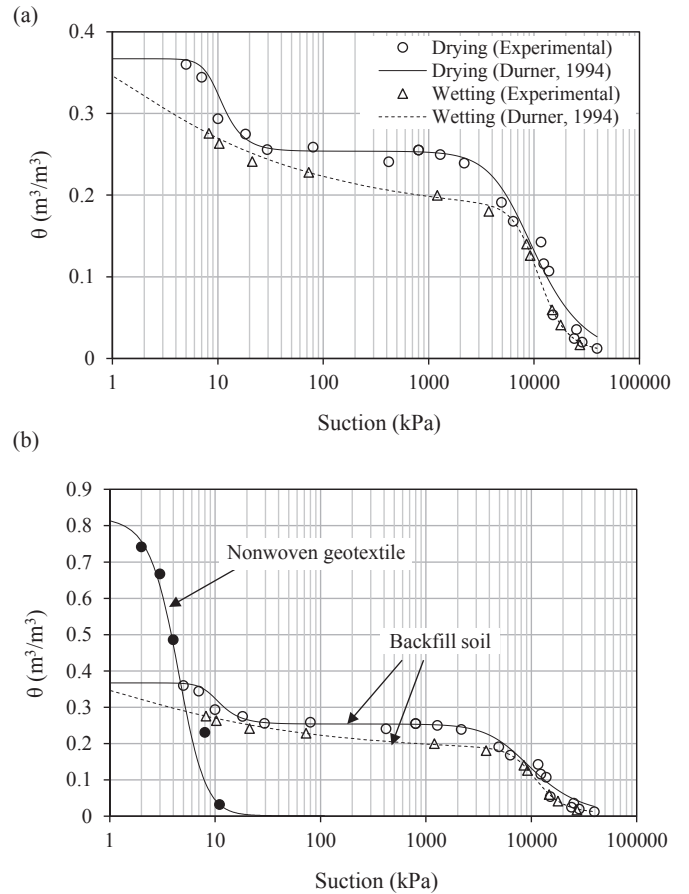


Fig. 1. Water retention curves: (a) Backfill soil by wetting and drying processes; (b) Geotextile (drying process).

are fitting parameters for the second segment. The fitting data is presented in Table 2.

A polyester needle-punched nonwoven geotextile was used as reinforcement. Table 3 summarizes the geotextile properties. Wide-width tensile tests were carried out in the longitudinal direction (i.e, the direction used for wall construction) following ASTM D4595 procedures. The hydraulic properties of the nonwoven geotextile, which are of particular relevance in this study, are also presented in Table 3. The geotextile water retention curve was obtained using desorption techniques following the procedures reported in ASTM D6836. Fig. 1b shows the geotextile water retention curve along with that of the backfill soil. The water retention curve of the nonwoven geotextile shows a highly nonlinear response, with a significant decrease in volumetric water content (or degree of saturation) within a comparatively narrow

Table 2
Properties of the nonwoven geotextile.

Parameter	Drying	Wetting
θ_s	0.36694 m ³ /m ³	0.39531 m ³ /m ³
θ_r	8.1447E-06 m ³ /m ³	6.5114E-07 m ³ /m ³
w_1	0.30842%	0.56463%
α_1	0.10855	1.7732
n_1	5.7777	1.2988
α_2	0.00014205	9.9828E-05
n_2	2.3648	3.8428
m_1	0.5	0.22
m_2	0.55	0.75

Table 3.
Properties of the nonwoven geotextile

Properties	Standard	Values
Weight per unit area	ASTM D5261	293 g/m ²
Thickness	ASTM D5199	2.96 mm
Permittivity	ASTM D4491	1.96 s ⁻¹
Transmissivity	ASTM D4716	6 × 10 ⁻⁶ m ² /s
Apparent opening size	AFNOR G38-017	93 μm
Tensile strength	ASTM D4595	12 kN/m
Elongation at failure	ASTM D4595	83%

range of suction. The air entry value and overall shape of this geosynthetic material is consistent with that reported in others studies (e.g. Stormont et al., 1997; Zornberg et al., 2010).

2.3. Characteristics of the full-scale reinforced soil wall

The geotextile-reinforced soil wall evaluated in this paper was constructed using backfill soil compacted to a 98% relative to the maximum dry unit weight using the standard Proctor effort. The target water content was reached by moisture conditioning the backfill soil before its placement and compacting it within the reinforced steel frame.

In order to achieve the target soil density, 50 mm-high soil layers were successively placed and compacted. Compaction control was achieved using the drive-cylinder method (ASTM D2937) in each compacted layer. A geotextile vertical spacing of 300 mm was adopted in this study. The soil and geotextiles layers were placed using a 1% inclination towards the facing to facilitate in-plane drainage. Each reinforcement layer was 1.60 m long, measured from the wall facing. After completed the layer compaction, the interfaces between soil and lateral metallic walls were filled with parafin in order to restrict the flow of water through interfaces. The cross section of the completed structure is

presented in Fig. 2, which shows the five reinforced layers (RL1, RL2, RL3, RL4 and RL5) of the structure. The wall was constructed using a wraparound facing, which involved no facing batter. A protective shotcrete facing, ranging in thickness from 50 to 80 mm was applied over the wrap-around facing of the reinforced soil wall. The shotcrete facing made of cement and sand (1:2) was adopted to simulate a typical protection system. Results of compressive strength tests of cylindrical specimens (ASTM C39/C39M) indicated 19 MPa of ultimate strength and 20 GPa of initial stiffness. Drainage geocomposites were used to facilitate drainage through the shotcrete facing panel, specifically located at the levels corresponding to the second and fourth reinforced layers (see Fig. 2). A view of the full-scale model after construction is presented in Fig. 3a.

2.4. Irrigation system

An irrigation system was installed over the geotextile-reinforced wall after its construction. The system includes a series of supply pipes and a drainage blanket placed on the top of the wall structure. The drainage blanket involved a 15 cm-thick sand layer overlain by a geocomposite drainage layer. The drainage blanket facilitated a uniform distribution of water over the wall surface. Water flow was supplied by a reservoir with a float switch used to maintain a constant hydraulic head. The magnitude of the irrigation rate was controlled by measuring the output volumetric flow in a water tap installed in the water reservoir. The interfaces soil-lateral walls at the top of the reinforced wall were filled with parafin in order to avoid the water flow and assure the infiltration of water through the soil. Fig. 3b and c provide details of the irrigation system and the drainage blanket.

2.5. Instrumentation

A comprehensive instrumentation program was conceived to

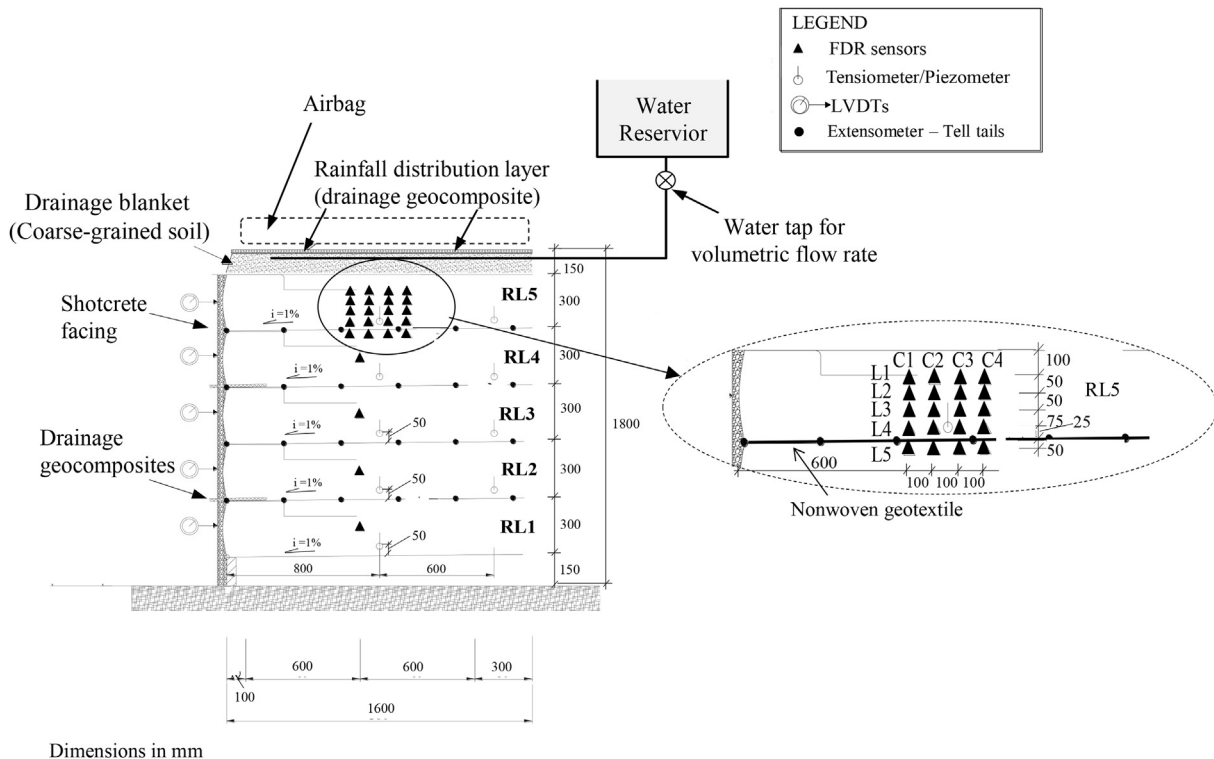


Fig. 2. Cross section of the full-scale wall, showing details of the irrigation system and instrumentation layout.

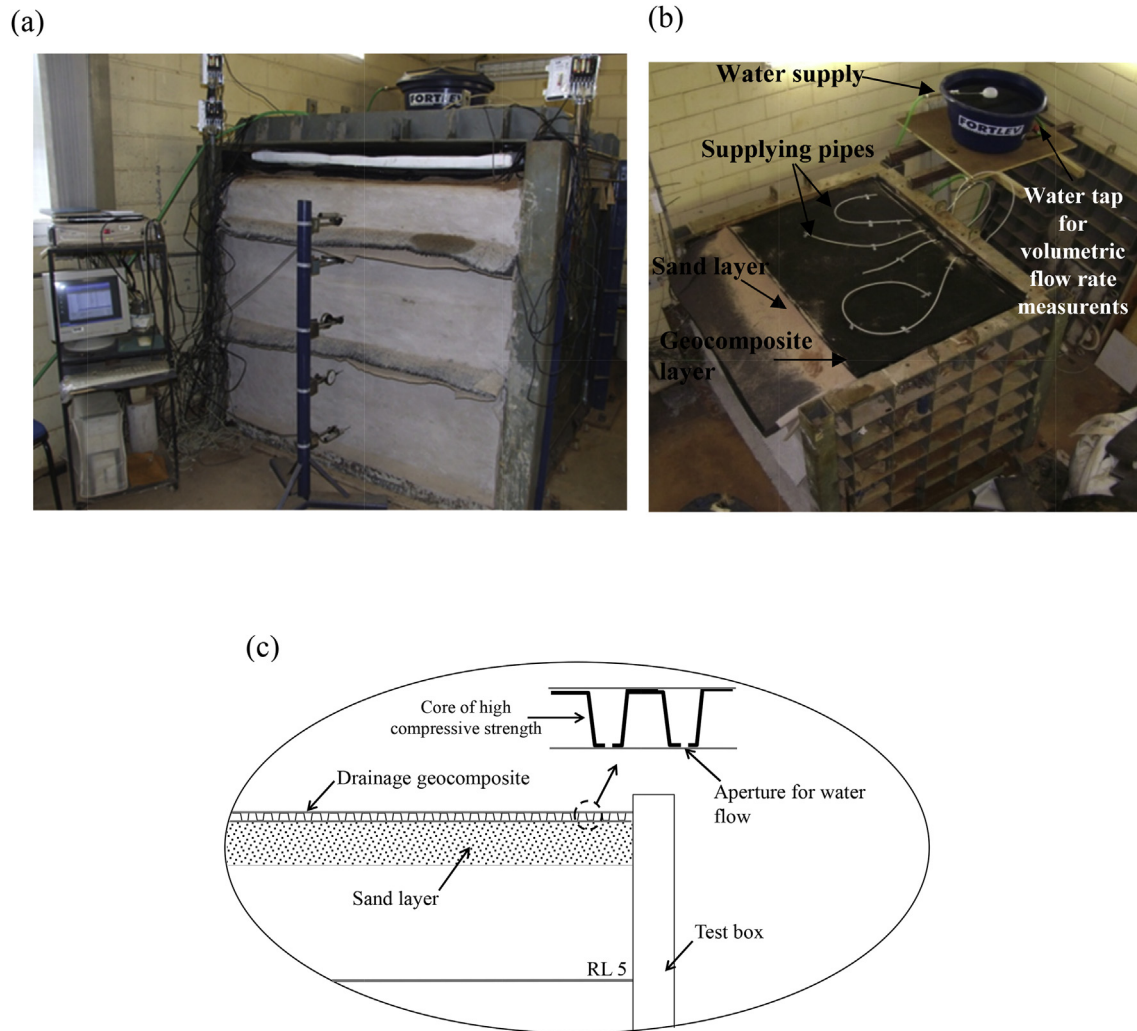


Fig. 3. View of the full-scale geotextile-reinforced wall: (a) Front view; (b) View of irrigation system; (c) Water distribution layer.

monitor pore water pressures (positive and negative) of soil, volumetric water content, reinforcement internal displacements and facing lateral displacements. The instrumentation layout is presented in Fig. 2.

The progress of water infiltration into the backfill soil was obtained using Frequency domain reflection (FDR) sensors installed to monitor the volumetric water content within each soil layer (placed 100 mm over each reinforcement layer). In addition, four vertical arrays of moisture sensors were installed on layer 5 (upper layer), in order to evaluate the development of a capillary break (Fig. 2). Piezometers that also allowed measurement of negative pore water pressures were also used to monitor changes in soil suction and development of pore water pressure during infiltration. The piezometers were placed 50 mm over each reinforcement layer and had a measurement range of -100 to 100 kPa.

The displacements at specific locations of the reinforcement layers were measured using mechanical extensometers (tell-tales). These devices consisted of stainless steel wires attached at different locations along the reinforcement. One end of each tell-tale was fixed to the geotextile and the opposite end was connected to a small weight used to tension the wires, facilitating the measurements of relative displacements. The steel wires were placed inside PVC tubes, which were used to minimize friction and to protect the wires. Displacements were monitored using linear variable

differential transformers (LVDTs) placed at the base of each weight. Fig. 2 shows the five points distributed along the length of each reinforcement layer. The points of measurements are located at the face and at 300, 600, 900, 1200 and 1500 mm from the face. Horizontal facing displacements were also measured using LVDTs located externally to the wall in the middle of each reinforced soil layer (Fig. 2).

2.6. Loading, irrigation and monitoring of the geotextile-reinforced wall

A surcharge loading of 100 kPa was applied before initiating irrigation using the airbag placed over the water distribution system. The metallic lid attached to the testing box lateral walls provided the necessary reaction. An irrigation rate of 1.8×10^{-7} m/s was applied uniformly over the full-scale model while maintaining the uniform surcharge of 100 kPa. Water ponding was not observed to occur on top of the wall, as the imposed impinging water flow was approximately 2.5 times smaller than the saturated hydraulic conductivity of the backfill soil. Data from the multiple instruments installed within the full-scale wall were simultaneously collected during loading and subsequent irrigation processes.

3. Monitoring results and analysis

3.1. Suction, moisture and capillary break

Fig. 4 shows the time history of the data obtained from the moisture sensors and piezometers located within the different reinforced soil layers (See Fig. 2). The volumetric water content corresponding to the saturation of soil was only observed in the moisture sensor located at 25 cm from the top of the wall (Layer RL5). As will be subsequently discussed, this sensor was able to capture the development of capillary break at this location. In the other layers (RL1 to RL4), where the moisture sensors were located at mid height of the reinforced soil layer, the increased water storage due to the development of a capillary break could not be detected at the sensor location. Fig. 4a also illustrates transient nature of the infiltration processes. Fig. 4b shows that the initial suction was reasonably uniform, ranging from 45 to 60 kPa. The water pressure readings show a sudden increase (i.e. a reduction of suction) as the infiltration front reached the location of the sensors. The maximum measured water pressure value reached in the sensors was approximately 0 kPa. The only exception was the reading of the piezometer installed 15 cm below the soil surface, which indicated positive pore water pressure values of up to 1.5 kPa. However, piezometers readings provided evidence that positive pore water pressures did not develop along the interface with the geotextile layers. As seen in Fig. 4b, the infiltration front reached the moisture sensors before reaching the tensiometers in

each of the soil layers. The tensiometers have been reported to require longer time to stabilize than the moisture sensors used in this research. Additionally, the moisture sensors are located above the tensiometers, which contributes to this behavior.

Fig. 4 demonstrates that tensiometers registered different values of water pressures at the beginning of the test, while the volumetric water content were registered as the same for all layers. It should be noted that VWC sensors used in the test are of FDR types, while the soil suction and pore water pressures were measured using tensiometers. Both dispositives of measurements are susceptible to some differences of measurement and inaccuracy. Additionally, the variability of compaction might be some source of inaccuracy. However, these inaccuracies do not affect the trends and correlations observed in this study.

Multiple vertical arrays of moisture sensors (four FDR arrays) were installed within the upper reinforced soil layer (RL5), as shown in Fig. 2, to evaluate the possible development of a capillary break. In each vertical array, four sensors were placed above the geotextile (L1, L2, L3 and L4) and one sensor was placed below the geotextile (L5). This configuration was adopted in order to observe the capillary break development and breakthrough. The time history of volumetric water content along each vertical array (C1, C2, C3 and C4) is shown in Fig. 5. The position of the various sensors is detailed in Fig. 2.

Fig. 5 provides the time history volumetric water content measured in the vertical arrays located at distances of 600, 700, 800 and 900 mm from the face, along reinforcement soil layer 5 (RL5).

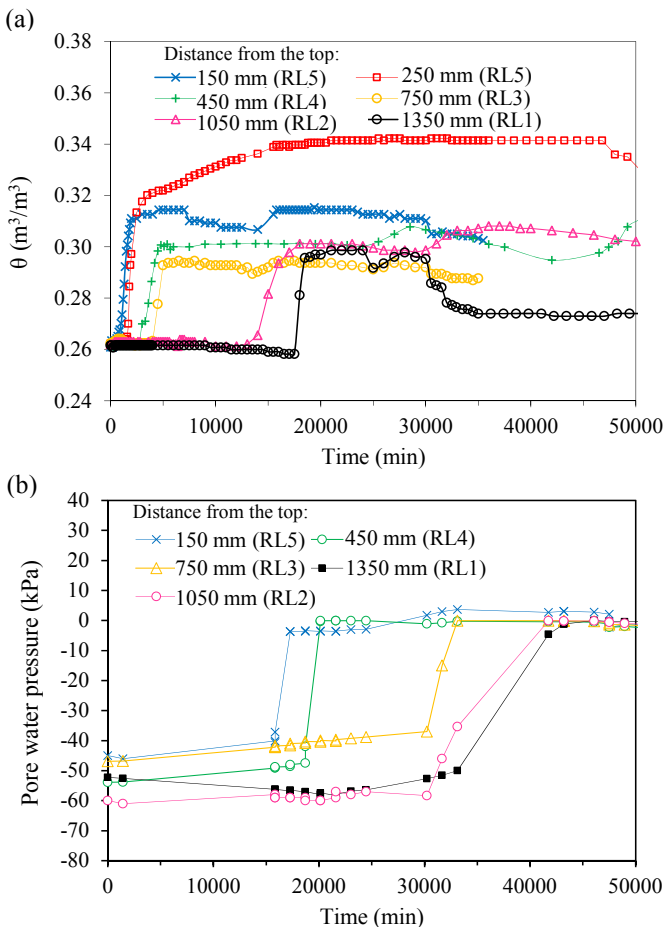


Fig. 4. Responses collected during infiltration for each reinforced layer (RL): (a) Volumetric water content and (b) Water pressure.

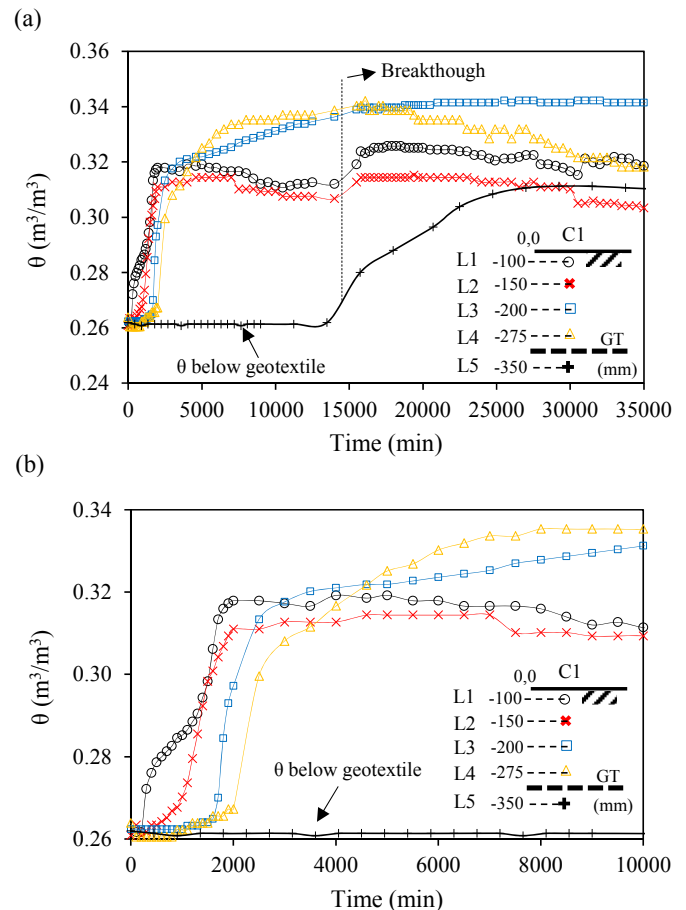


Fig. 5. Volumetric water content measured in the vertical arrays C1 in the upper reinforced soil layer: (a) until 35,000 min and (b) until 10,000 min of test.

As previously mentioned, the geotextile was sloped at 1% toward the facing, which may have facilitated moisture migration towards the sensors located close to the face. As recorded by the volumetric water content sensors shown in Fig. 5a, three distinct phases of moisture response can be identified after applying a constant infiltration rate of 1.8×10^{-7} m/s. Initially, the entire profile was relatively dry, with an as-compacted volumetric water content of 0.262 that corresponds to the initial volumetric water content (θ_i). The advancing wetting front is a transient infiltration process that results from applying a constant impinging flow rate. As the wetting front reaches the location of each sensor, the volumetric water content is observed to increase from θ_i to a value of approximately 0.310 that corresponds to the equilibrium volumetric water content for this condition (θ_{eq}). After the wetting front reached the top of geotextile (around 3000 min after testing initiation), the water did not immediately flow into the geotextile. Instead, a capillary break developed and water accumulated within the soil immediately above the geotextile reinforcement. Such accumulation continued until the suction decreased to a comparatively low value, when breakthrough occurred (approximately 15,000 min after test initiation). Due to the development of a capillary break, the volumetric water content reached a value of approximately 0.34, which corresponds to soil saturation (θ_{sat}). The results obtained in Fig. 5 were found to have similar experimental trends to those observed in McCartney et al. (2005) and McCartney and Zornberg (2010). The capillary break development along the vertical arrays C2, C3 and C4 showed similar volumetric water content responses to those observed for vertical array C1, although with slight changes in the periods of capillary break development and breakthrough. This is the motivation of not presenting results for C2, C3 and C4 arrays.

As a result of the development of the capillary break in RL5, observed in all vertical arrays (Fig. 5), infiltration into RL4 (the second layer from the top) was delayed. Specifically, the development of the capillary break led to a 4 days (6000 min) retardation of the infiltration per reinforcement layer, until the suction decreased to the breakthrough value. At this point, the geotextile became more permeable than the soil and downward flow occurred. According to the moisture data presented in Fig. 5, the breakthrough suction corresponds to a volumetric water content value of $0.33 \text{ m}^3/\text{m}^3$. In this study, the breakthrough suction could not be measured directly, as the tensiometers were not positioned immediately above the geotextile. However, the breakthrough suction was found to range from 6 to 10 kPa, which corresponds to suction value obtained from the SWRC (Fig. 1) using the breakthrough water content. After breakthrough, water advanced into the underlying layer and the volumetric water content in the RL5 was observed to reduce to that corresponding to the equilibrium water content (θ_{eq}).

According to Zornberg et al. (2010), the breakthrough suction corresponds to the value for which both the backfill soil and the geotextile have the same unsaturated hydraulic conductivity value. Fig. 6 illustrates the hydraulic conductivity functions (k-functions) of the geotextile and the backfill soil used in the full-scale walls. These curves were obtained using the data from water retention curves for both materials (Fig. 1) to develop fitting parameters for the van Genuchten model in the first segment of the SWRC (van Genuchten, 1980; Mualem, 1976). As indicated in Fig. 6, the breakthrough suction defined by the intersection of the hydraulic conductivity functions is approximately 20 kPa. The hydraulic functions observed in this study were observed to be similar to those observed in Bouazza et al. (2013). Comparison of the breakthrough suction values obtained from the monitored volumetric water content data (Fig. 5) and from the k-functions of both materials (Fig. 6) result in comparatively similar values.

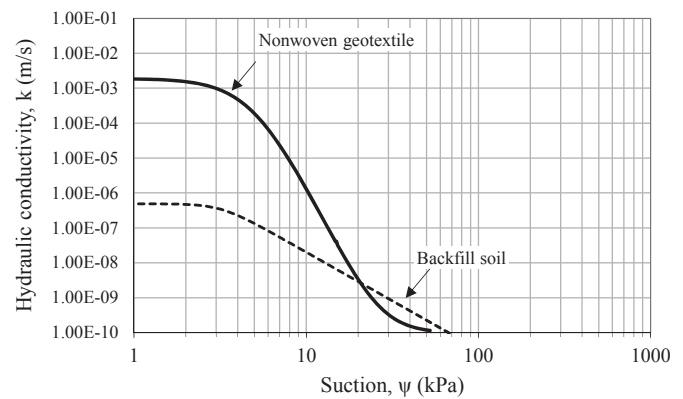


Fig. 6. K-functions of backfill soil and nonwoven geotextile.

A comparison between the total water volumes imposed and measured during infiltration is presented in Fig. 7. The imposed water volume was defined considering the actual flow rate applied as irrigation during the test. That is, it was assumed that the entire volume of water imposed as irrigation ultimately infiltrated into the backfill soil. The volume of water infiltrated during the test was also predicted considering the changes in water storage within the backfill soil, as measured by moisture sensors. The results show that there is practically no change in the measured infiltration during the period ranging from 1500 to 11,000 min, which can be attributed to a restricted infiltration due to the development of a capillary break. After this period, the breakthrough of water is reached and the infiltration is retaken. The difference between imposed and infiltrated flow rates observed in Fig. 7 provide an estimate of the amount of water drained through the geotextile during the test (approximately 0.25 m^3). Additionally, the results indicate that water drained primarily within through the top geotextile layer, in which imposed and measured flow rate values were found to be similar after 10,000 min of the test. It should be noted divergencies between the imposed flow and measured infiltration in the beginning of the curve in Fig. 7, which was not expected. These divergencies can be attributed to the inaccuracy of FDR sensors used to capture the volumetric water content, since these types of sensors are sensible to the variability of compaction.

Fig. 8 shows a view of the facing of the full-scale geotextile reinforced wall after 20,000 min of irrigation. The picture illustrates that moisture stained the facing at the elevation of the reinforcement layers, with concentrated moisture stains in the elevations of layers RL4 and RL5 (upper layers). This may be attributed to the in-

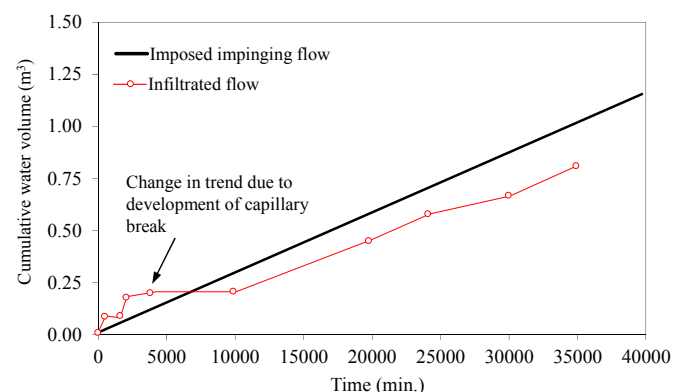


Fig. 7. Cumulative water volumes into the reinforced soil wall.

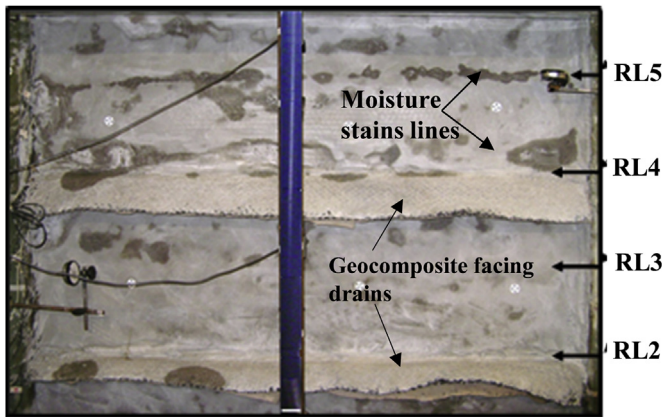


Fig. 8. Front view of the reinforced soil wall model after 10,000 min of test initiation.

plane drainage capacity of the nonwoven geotextile reinforcements after capillary breakthrough. The fact that there are moisture stains at all of the layers implies that there is breakthrough of the upper layers into the lower layers. These observation corroborate the large quantity of water drained by the upper layer obtained in Fig. 7.

3.2. Analysis of moisture profiles

Considering the three distinctive volumetric water content values defined at the different stages during infiltration (θ_i , θ_{eq} , θ_{sat}), moisture profiles could be defined for different periods throughout the infiltration test. Three distinctive values of water contents were also observed in the infiltration columns evaluated by McCartney and Zornberg (2010). Determination of these distinctive volumetric water content values allows defining the moisture profile along the entire height of the wall using the volumetric water content measurements that have only been collected in a limited number of locations across the structure height. Fig. 9 illustrates the moisture profiles corresponding to times 2000 min, 10,000 min and 30,000 min. Volumetric water content data allowed the definition of an infiltration front (solid

lines) for each monitored stage in this study.

Suction profiles could also be defined using the piezometer/tensiometer readings and the water retention curve of the soil. Fig. 10 shows the suction profiles for the same three different periods of the test evaluated in Fig. 9. Three distinctive suction values can be identified: Initial (ψ_i), equilibrium (ψ_{eq}), and saturation (ψ_{sat}), corresponding to 45, 8 and 0 kPa, respectively.

Fig. 11 presents the time history of the depth of the infiltration front into the reinforced soil mass obtained using the moisture and suction profiles shown in Figs. 9 and 10. The expected progress of infiltration front if capillary breaks would not develop are compared in Fig. 11 against the actual infiltration time histories as affected by the presence of reinforcements. As the upper soil layer was more extensively instrumented with moisture sensors, the infiltration rate could be more precisely captured and the phenomena occurring at the interface could be better described. The infiltration front expected in the unreinforced soil was obtained by extrapolating the hydraulic behavior captured in the upper soil layer, before reaching the elevation of the reinforcement layer. The infiltration front in the reinforced soil (with geotextiles layers) was obtained by extrapolating the hydraulic behavior occurring in the upper layer considering the presence of the reinforcement, i.e. the time-depth of infiltration front curve between immediately above 300 mm to immediately above 600 mm were repeated for further depth. It was made in order to account for the development of capillary break in all reinforced layers. In other words, the interface phenomenon captured in the upper soil layer was also assumed to occur in the other reinforcement layers. In Fig. 11, the infiltration front of the unreinforced soil was expected to reach the base of the wall in 10 days (approximately 10,000 min into the test). However, the actual infiltration to the base of the reinforced soil structure was completed in approximately 30 days. The difference evidences the effect that the presence of nonwoven geotextile reinforcements has on retarding infiltration.

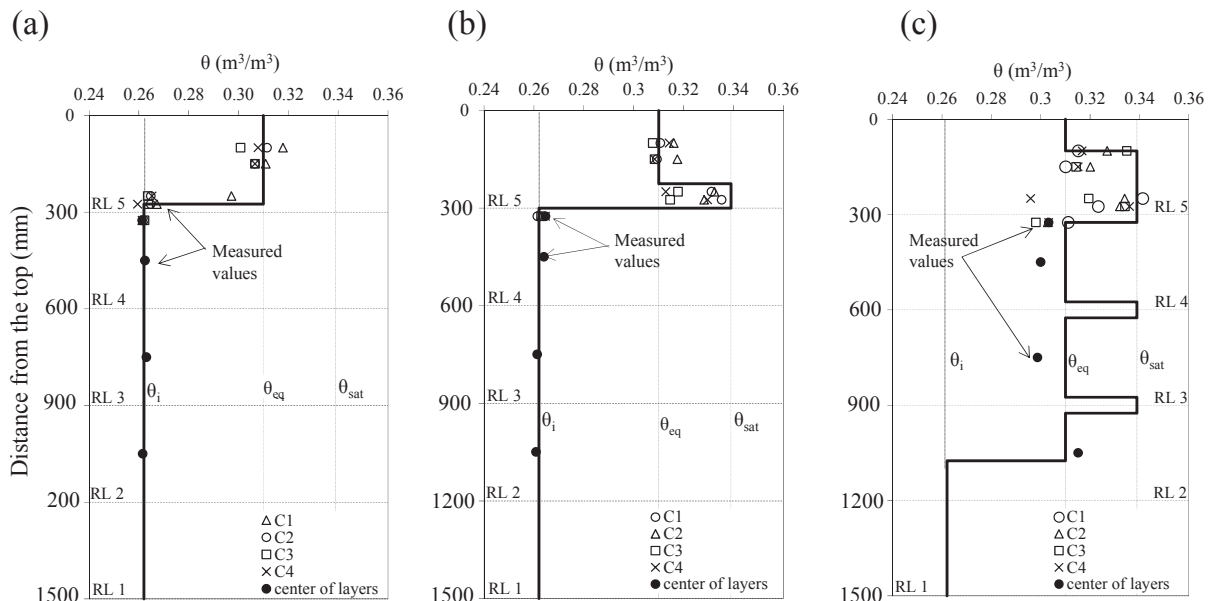


Fig. 9. Moisture profiles after: (a) 2000 min, (b) 10,000 min and (c) 30,000 min of test initiation.

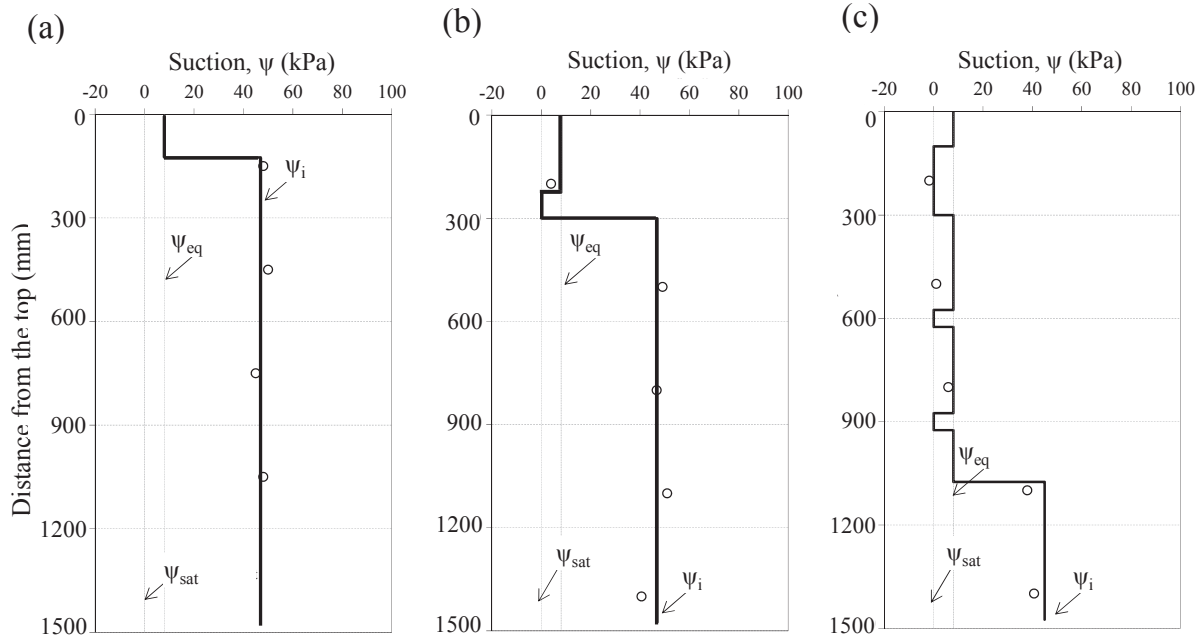


Fig. 10. Suction profiles after: (a) 2000 min, (b) 10,000 min and (c) 30,000 of test initiation.

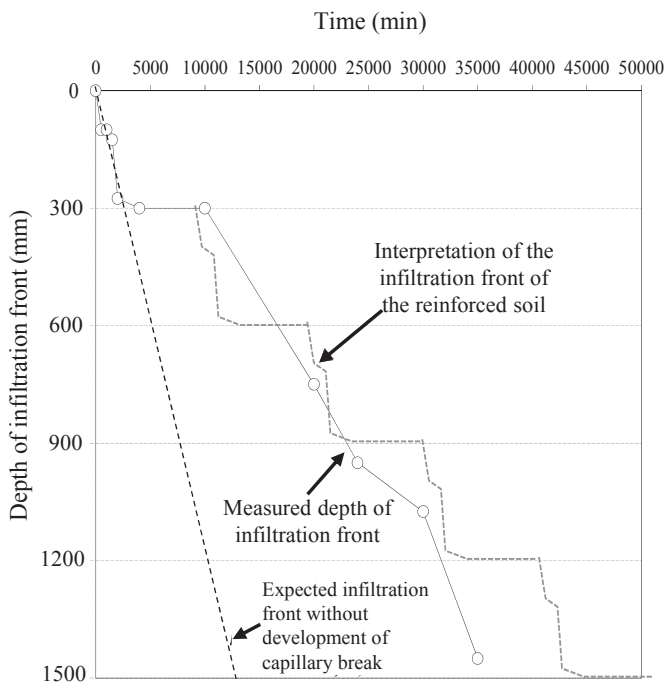


Fig. 11. Time history of the depth of infiltration front based on measured sensors responses.

4. Effect of water infiltration on the wall performance

4.1. Behavior of the reinforced soil wall

The effect of infiltration on wall performance was assessed by evaluating the monitored displacements along geotextiles as well as the external facing displacements. The reinforcement strains were defined using the displacements measurements. As indicated

in Fig. 2, displacements were monitored at 5 different locations along the geotextiles. Specifically, displacements were measured at points located 300, 600, 900, 1200 and 1500 mm from the wall facing. Results of internal displacements (δ_i) measured in layers RL5, RL4, RL3 and RL2, as a function of time, are shown in Fig. 12. Fig. 12a correspond to the upper layer (RL5) and illustrate the development of high level of internal displacements in comparison to the layers below. The time history of internal displacements also show a significant increase after 30,000 min. This period corresponds to the time when the infiltration front advanced past the RL2 (1200 mm from the top), which means the infiltration front had advanced past half of the structure. As expected, the internal displacements along the reinforcements are higher in locations closed to the facing (300 and 600 mm), with decreasing displacements towards the back of the wall.

Fig. 13 provides an example of reinforcement strains obtained using a sigmoidal fitting of the relative displacements (for layer RL3). The distribution of relative displacements along the RL3 is presented in Fig. 13a. In this figure, sigmoid curves were defined to fit the raw displacement data in order to obtain a smooth representation of the distribution of displacements along the reinforcement length (Fig. 13a). The displacement function can then be used to obtain the distribution of strains along the reinforcement length, using the procedure discussed by Zornberg and Arriaga (2003). Geotextile strains have often been reported by calculating the relative displacements between consecutive mechanical extensometers (tell-tales) and dividing them by the initial distance between points of measurement. However, this technique often leads to significant scatter, particularly if the distance between measurement points is comparatively large. Consequently, the raw data from extensometer displacements was initially smoothed by fitting the data to a sigmoidal function. Then, the distribution of strains along the geotextile length was obtained as the derivative of the displacement function. Fig. 13b shows an example of the strain distribution (for layer RL3). This same approach was used in this study to assess the geotextile strains in all reinforcement layers. In order to analyze the impact of infiltration on wall performance, the

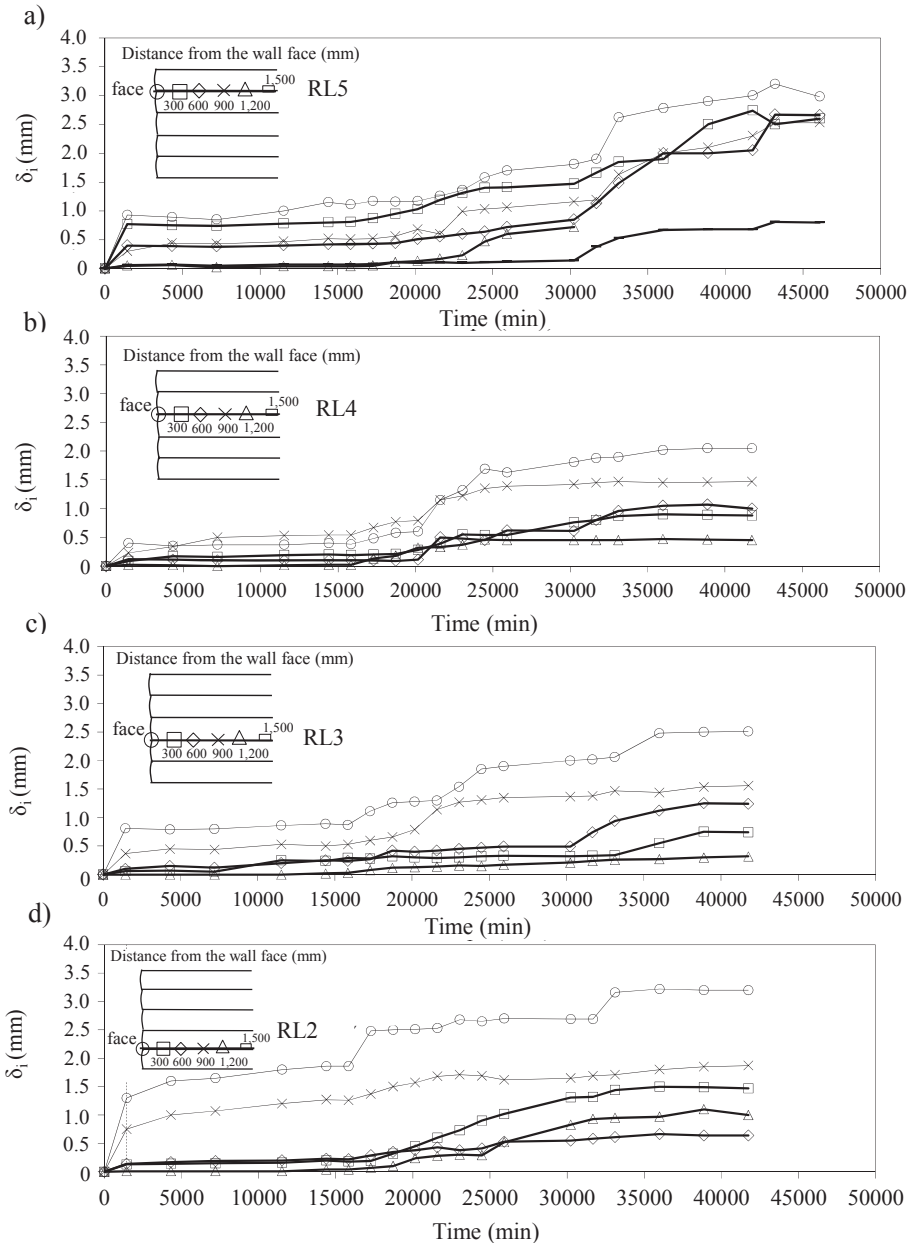


Fig. 12. Displacements along the geotextile reinforcements during the infiltration in reinforcement layers: (a) RL5, (b) RL4, (c) RL3 and (d) RL2.

peak reinforcement strains (ϵ_{peak}) were obtained at relevant time throughout the test.

Fig. 14 shows the time history of the reinforcement peak strains (ϵ_{peak}) and of the volumetric water content (θ) monitored throughout the test. In the case of the RL5 (upper layer), which included a denser array of moisture sensors, the sensor located at 12.5 cm from the geotextile (Fig. 2) was adopted for this evaluation. For the remaining layers, only one sensor per layer was installed, which was used in this evaluation. The times corresponding to the initial development of the capillary break and to the subsequent breakthrough are also indicated in Fig. 14 in order to evaluate the possible impact of water storage on the wall performance. In general, the strain results show that increases in volumetric water content tend to lead to increases in the maximum reinforcement strain (ϵ_{max}). However, the increases in ϵ_{peak} seems to be more strongly related to the advancement of the infiltration front into the

unsaturated soil mass. For example, the results in Fig. 14a indicate that times with significant moisture changes in RL5 do not necessarily correspond to the times with significant increases in reinforcement strains. Instead, the significant increases in reinforcement strains are more evident when the infiltration front has advanced into the underlying reinforcement layer. The moisture increase (capillary break) and subsequent breakthrough of the lower layers are also observed to lead to increases in reinforcement strains. However, the moisture accumulation in top layers is observed to result in increases in geotextile strains in the multiple lower layers. Accordingly, the time history of the lower reinforcement layers show multiple periods of strain increases.

Fig. 15 presents the time history of the monitored facing displacements (δ_{face}) and of the volumetric water contents monitored throughout the test. A maximum facing displacement of 1.5 mm was recorded in RL2 (Fig. 15d) towards the end of the test. In

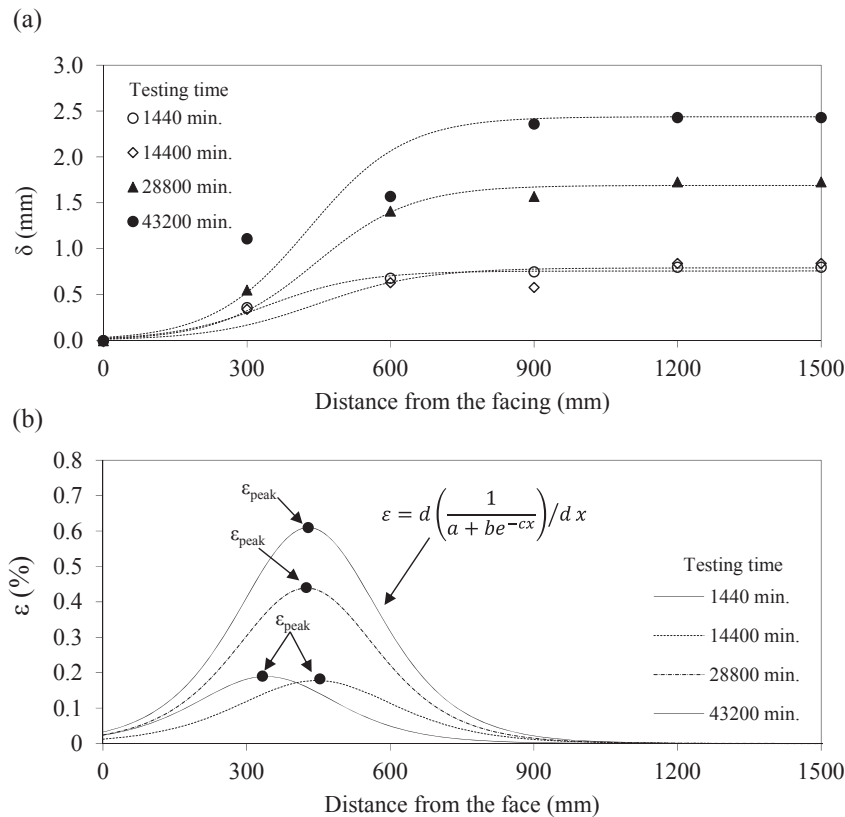


Fig. 13. Geotextiles displacements in Reinforced Layer 3: (a) Sigmoidal function fitting of relative displacement data; (b) Predicted geotextile strains distribution.

general, increases in face displacements are related to increases in volumetric water content. Fig. 15a indicates that significant increases in displacements only occurred when infiltration advances to the lower soil layers of the reinforced soil wall. This is consistent with the previously discussed strain time history. In RL4 (Fig. 15b), increases in displacements due to moisture increases are observed to be slightly higher than those in the RL5 (Fig. 15a). Similarly, the increases in displacements in RL3 and RL2 were higher than those observed in the upper layers with face movements occurring before the arrival of the wetting front (Fig. 15c and d). This indicates that advancement of the moisture front and corresponding progressive loss in suction, can result in lateral movements in layers below the moisture front location due to the global reduction of soil mass stiffness. This is better illustrated in Fig. 16a, which allows assessment of the effect of the infiltration front on the maximum facing displacement (δ_{\max}), recorded at any given time during the test. Also, Fig. 16b shows the effect of infiltration on maximum peak reinforcement strain (ϵ_{\max}) obtained at any given time among all reinforced layers. The results show that the depth of the wetting front correlates well with the maximum peak reinforcement strain (ϵ_{\max}), as well as maximum facing displacement. That is, increases in facing displacements and in reinforcement strains were found to be correlated more strongly to the depth of the moisture front than to increases in soil moisture values.

4.2. Stability analysis of the reinforced soil wall

The effect of infiltration on the calculated factor of safety (FOS) was also evaluated in this research. The factors of safety were obtained using Spencer's method of limit equilibrium analysis, accounting for both reinforcement contribution and the negative and/or positive pore water pressures within the reinforced soil mass.

Additionally, the weight of the shotcrete facing was considered in the stability analysis. The shear strength of the shotcrete facing was not considered in the stability analysis, since surface failures passing at the toe of the reinforced soil model was assumed. Therefore, no significant contribution of the shear strength of the shotcrete facing is expected in the stability analysis. The calculated factors of safety (FOS) also accounted for changes in backfill soil unit weight due to changes in soil volumetric water contents during infiltration. The measured suction values were used as input for these analyses. The effect of suction reduction on the drained cohesion of the soil was also considered as proposed by Fredlund et al. (1978). Circular critical failure surfaces were adopted for the analyses (Fig. 17). Soil strength from CD triaxial tests (Table 1) and geotextile tensile strength from wide-width tensile tests (Table 2) were used in these analyses. Fig. 17 shows the location of the critical failure surfaces, obtained using limit equilibrium analyses, as well as the location where peak strains (ϵ_{peak}) occurred in each reinforced layer at different times. As shown in the figure, the predicted critical slip surfaces are consistent with the location where peak strains occurred. Also, the shape of slip surfaces was not significantly affected by infiltration.

The calculated factors of safety and maximum reinforcement peak strains (ϵ_{\max}) from displacement measurements are plotted in Fig. 18 as function of the cumulative water volume imposed during the test. The results indicate that increasing cumulative water volumes lead to a clearly decreasing trend in the FOS and to an increasing trend in the maximum geotextile strain. Although the cumulative water infiltration correlates to the FOS, the cumulative volume of infiltration appears not to be a good index to characterize the effect of infiltration on deformability (e.g. ϵ_{\max}) and face displacements in view of the scattering of points in the linear fitting. Additionally, the relation between FOS and cumulative water

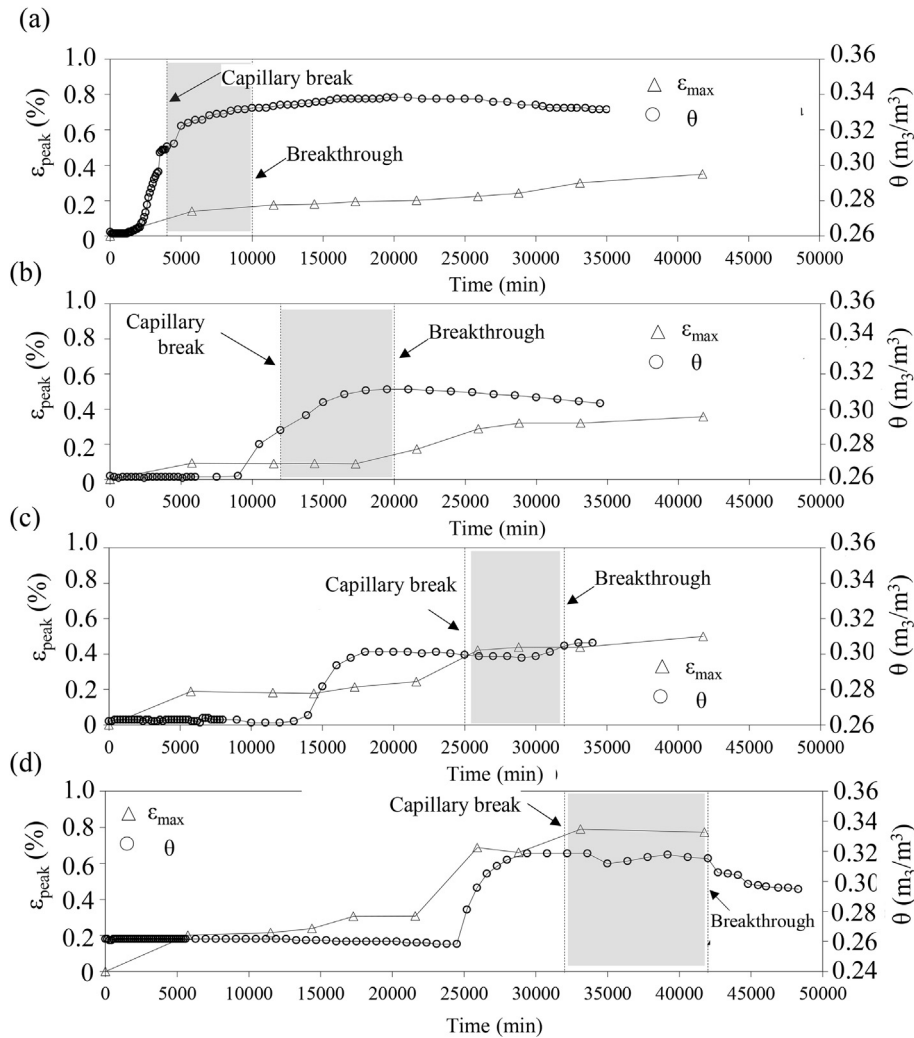


Fig. 14. Geotextile peak strains (ϵ_{max}) during the infiltration on reinforcement layers: (a) RL5, (b) RL4, (c) RL3 and (d) RL2.

infiltration seems not to be linear since the two first points of the curve have shown no alteration in FOS with increasing of water infiltration.

Fig. 19 shows the calculated FOS as a function of the average of suctions measured by the tensiometers installed at different locations within the geotextile-reinforced soil wall (See Fig. 2). Also, the maximum facing displacements (δ_{max}) (Fig. 19a) and the maximum peak reinforcement strains (ϵ_{max}) (Fig. 19b) are related to the average of suction. The trends indicate that ϵ_{max} decreases while FOS increases with increasing average suction, while δ_{max} increases and FOS decreases with decreasing average suction. The trends also indicate that δ_{max} increases with decreasing average suction. Interestingly, the trends were found to be bilinear. Clearly, reinforcement strains and face displacements were found to reduce more significantly with reduction of suction until a certain value of suction (45 kPa) from which the rate of decreasing declines. Similar behavior was observed when FOS is related to the average of suction, the FOS starts to decrease with suction reduction from which a certain value of suction. Before this value, the FOS was found not to change. Similarly, Marinho et al. (1995) have reported that the shear modulus of compacted sample of soil increases until a certain value of suction from which no significant increases in modulus is reached. These observations suggest that average of suctions is a relevant parameter to characterize the effect of infiltration on both

the stability and deformability of unsaturated geotextile-reinforced soil walls subjected to infiltration. The results shown in Fig. 19 indicate that a saturated condition (zero suction) for the backfill soil corresponds to a factor of safety of 1.6, a maximum peak strain of 1.6% and a maximum facing displacements of 2.6 mm.

Fig. 20 relates the FOS, ϵ_{max} and δ_{max} to the average of degree of saturation during infiltration. In this evaluation, the average of degree of saturation was calculated using the response of moisture sensors installed at different locations along the structure (See Fig. 2) over all measured values at a time. Average values of degree of saturation and suction are subjected to the locations of the moisture sensors (See Fig. 2). The parameters ϵ_{max} and δ_{max} show a linear increasing trend with increasing average of degree of saturation. However, the FOS was found to increase with increasing value of average degree of saturation (as observed for ϵ_{max} and δ_{max}) with different rates of increasing, resulting in a bilinear trend. Accordingly, the average degree of saturation appears not to be a better choice than the average soil suction for use as an index parameter to capture both stability and deformability.

5. Conclusions

A full-scale geotextile-reinforced soil wall was built in a laboratory setting in order to assess the effect of water infiltration on

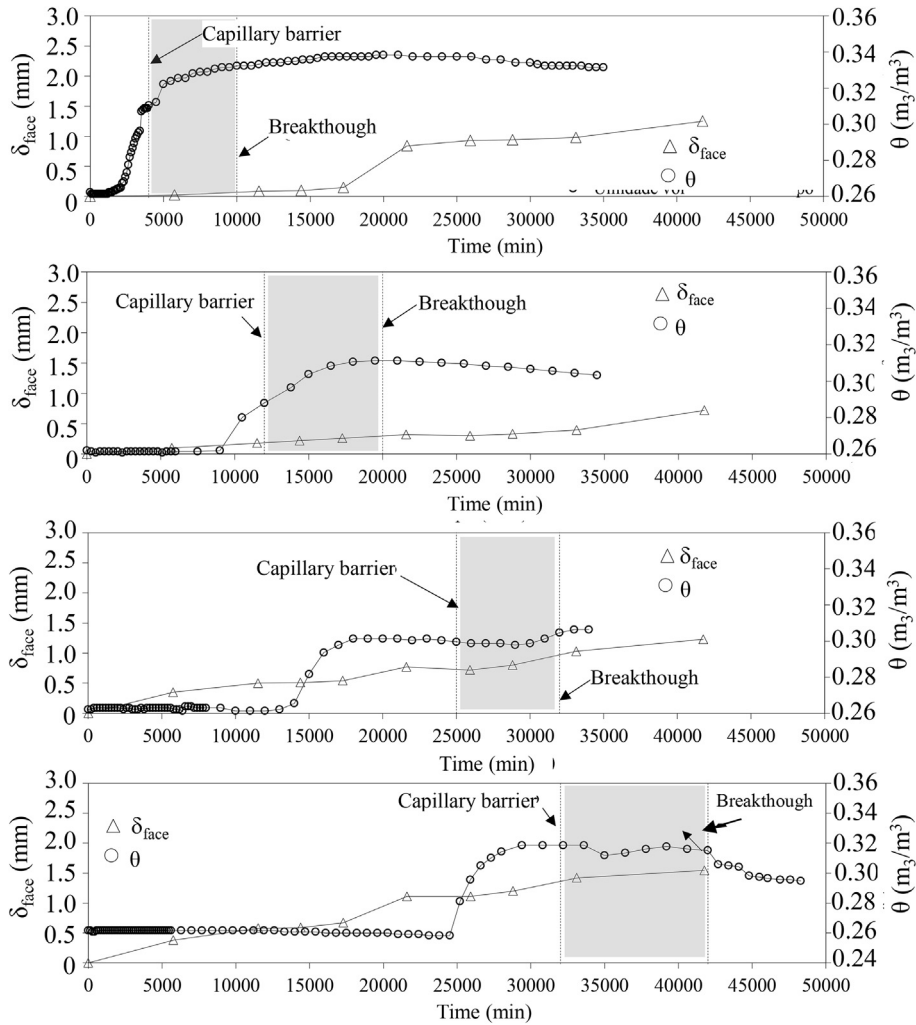


Fig. 15. Facing displacements (δ_{face}) during the infiltration on reinforcement layers: (a) RL5, (b) RL4, (c) RL3 and (d) RL2.

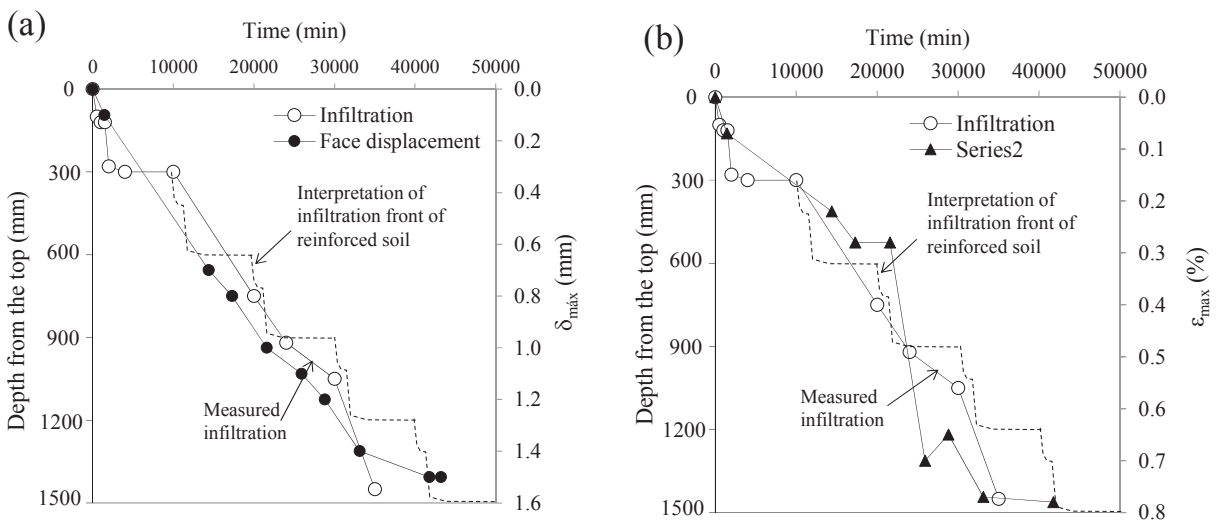


Fig. 16. Effect of advancement of infiltration front on: (a) Maximum geotextile strains, and (b) Maximum facing displacements.

the overall performance of the structure. Nonwoven geotextiles were selected as inclusions in order to provide not only

reinforcement, but also internal drainage to the fine-grained soil used as backfill material. An irrigation system was used in order to

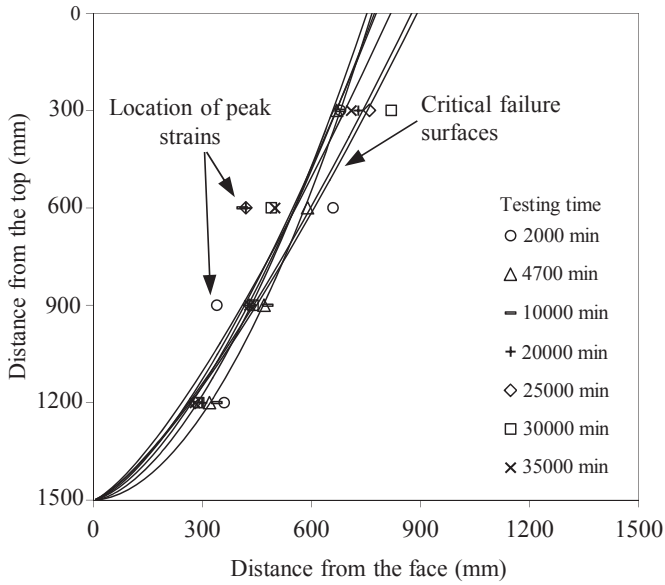


Fig. 17. Critical failure surfaces from limit equilibrium analyses of the reinforced soil wall during test.

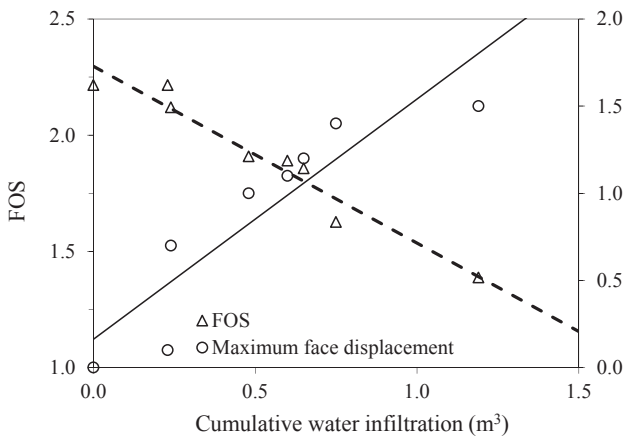
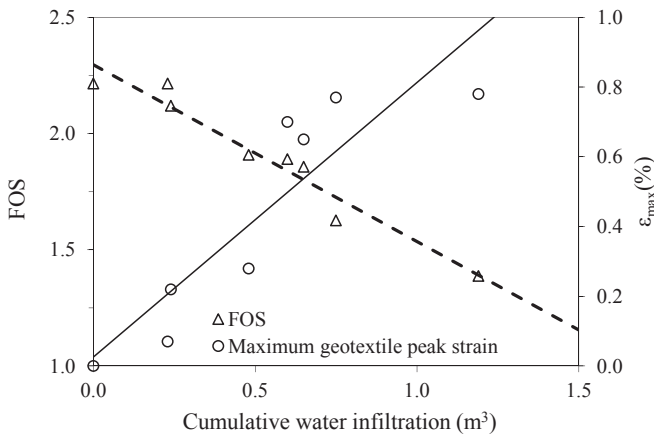


Fig. 18. Effect of cumulative water infiltration on factor of safety and geotextile maximum peak strains (ϵ_{max}).

simulate rainfall events. The test was conducted under a constant irrigation rate and surcharge of 100 kPa. The instrumentation

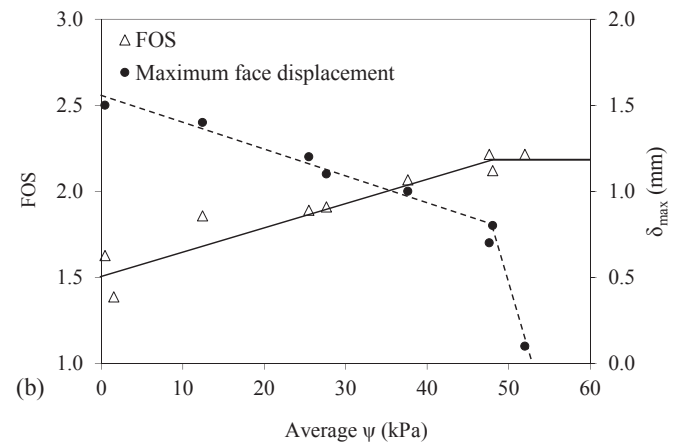
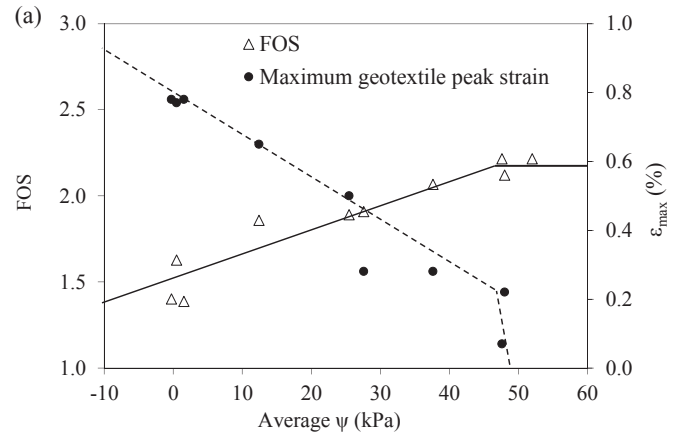


Fig. 19. Effect of average suction increases on factor of safety and: (a) Maximum facing displacements (δ_{max}) and (b) Geotextile maximum peak strains (ϵ_{max}).

program allowed evaluation of advancement of the infiltration front, internal geosynthetic drainage and the development of a capillary break. In addition, the wall deformability was also monitored during infiltration. The following conclusions can be drawn from analysis of the experimental results obtained in this study:

- Capillary breaks were found to develop during infiltration at the interface between the backfill soil and the nonwoven geotextiles. The development of capillary breaks was found to retard the infiltration process for the conditions in this study, retardation was 4 days per reinforced layer. Specifically, the infiltration front was observed to reach the bottom of the geotextile-reinforced soil wall after approximately 30 days of irrigation, On the other hand, the infiltration front was expected to reach the base of the wall in approximately 10 days without the development of capillary breaks.
- Nonwoven geotextiles were found not to provide internal drainage to the reinforced wall during the initial development of the capillary break. However, after breakthrough, nonwoven geotextiles were found to provide the internal drainage, which diverted approximately 25% of the water volume. Moisture stains in the wall facing at the locations of the geotextiles layers indicated that the most of internal drainage occurred through the upper reinforcement layers.
- The set of moisture sensors allowed identifying three distinctive values of volumetric water content during infiltration processes: the initial (as compacted volumetric water content); second, an

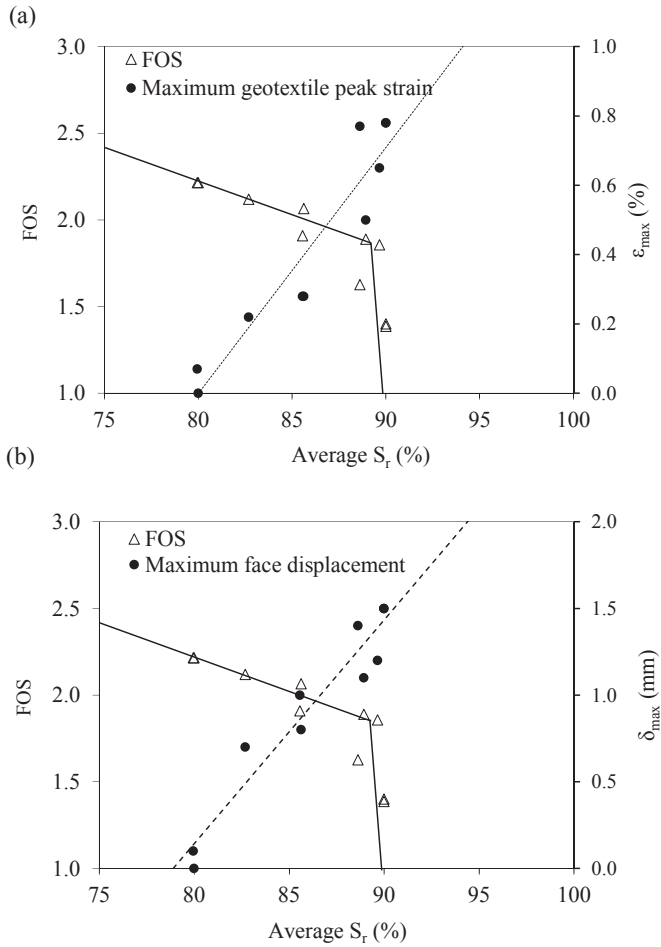


Fig. 20. Effect of average of degree of saturation increases on factor of safety and: (a) Maximum facing displacements (δ_{max}) and (b) Geotextile maximum peak strains (ϵ_{max}).

equilibrium volumetric water content; and the saturation volumetric water content. The determination of these distinctive volumetric water content values facilitated defining the moisture profile along the entire height of the wall.

- While generation of positive pore water pressure was not evidenced during the test, the advancing infiltration front was found to affect the performance of the wall. Specifically, infiltration led to significant increases on reinforcement strains and face displacements. In, particular, the moisture increase due to capillary break and subsequent breakthrough were observed to lead to increases in reinforcement strains. The moisture accumulation in top layers, which resulted in an increase in unit weight of the soil, is observed to result in increases in geotextile strains in the multiple lower layers. Additionally, the time history of geotextile strains, particularly in the lower reinforcement layers, showed multiple periods of strain increases.
- The depth of the infiltration front was found to correlate well with the maximum peak reinforcement strains, as well as with the maximum facing displacements. That is, increases in facing displacements and reinforcement strains of the geotextile-reinforced soil wall were found to be more strongly related to the depth of moisture front than to increases in soil moisture.
- Reinforcement strains and face displacements were found to reduce more significantly with reduction of suction until a certain value of suction (45 kPa) from which the rate of

decreasing declines. Similar behavior was observed when FOS is related to the average of suction, the FOS starts to decrease with suction reduction from which a certain value of suction. Before this value, the FOS was found not to change. Accordingly, average suction was found to be a suitable parameter to assess the effect of infiltration on the stability and deformability of unsaturated geotextile-reinforced soil walls subjected to infiltration.

Acknowledgements

The authors specially acknowledge the late Professor Benedito de Souza Bueno for his significant contribution to this study. The authors wish to thank the University of Sao Paulo for the availability of their facilities and funding provided by FAPESP (2015/05807-5).

Notations

Basic SI units given in parentheses

G_s	Soil specific gravity (dimensionless)
θ	Volumetric water content (m^3/m^3)
θ_i	Initial volumetric water content (m^3/m^3)
θ_{eq}	Volumetric water content at equilibrium (m^3/m^3)
θ_{sat}	Volumetric water content of saturated soil (m^3/m^3)
u	Pore water pressures (kPa)
ψ	Suction (kPa)
ϵ	Reinforcement strains (%)
ϵ_{peak}	Reinforcement peak strains (%)
ϵ_{max}	Maximum reinforcement peak strains (%)
δ	Displacement (in mm)
δ_{max}	Maximum displacement (in mm)
δ_i	Internal reinforcement displacements (mm)
δ_{face}	Wall facing displacements (mm)
i	Inclination (degree)
S	Degree of saturation (degree)
k	Hydraulic conductivity (m/s)

Abbreviations

GRS	Geosynthetic-reinforced soil
CD	Consolidated Drained
FDR	Frequency Domain Reflectometer
FOS	Factor of Safety
CU	Consolidated Undrained triaxial compression test
RL	Reinforced soil layer
LVDT	Linear variable differential transformer
VWC	Volumetric water content
WC	Water content
V	Volume
C1	Sensor column (vertical array) 1
C2	Sensor column (vertical array) 2
C3	Sensor column (vertical array) 3
C4	Sensor column (vertical array) 4
L1	Sensor line 1
L2	Sensor line 2
L3	Sensor line 3
L4	Sensor line 4

References

AASHTO, 2002. Standard Specifications for Highway Bridges. Div. 1, Sect. 5, Retaining Walls, seventeenth ed. American Association of State Highway and Transportation Officials, Washington, DC, USA. 89pp.
 ASTM C39/C39M, 2016. Standard Test Method for Compressive Strength of Cylindrical Concrete Specimens. ASTM International, West Conshohocken, PA, USA.

- ASTM D2937, 2010. Standard Test Method Density of Soil in Place by the Drive-Cylinder Method (West Conshohocken, Philadelphia, USA).
- ASTM D422-63, 2011. Standard Test Method for Particle-size Analyses of Soils. West Conshohocken, Philadelphia, USA. p.8.
- ASTM D4595, 2011. Standard Test Method for Tensile Properties of Geotextile by the Wide-width Strip Method (West Conshohocken, Philadelphia, USA).
- ASTM D1557, 2009. Standard Test Methods for Laboratory Compaction Characteristic of Soil Using Modified Effort. American Society of Testing Materials, p. 14.
- ASTM D7181, 2011. Method for Consolidated Drained Triaxial Tests for Soils. American Society of Testing Materials, p. 11.
- ASTM D5261, 2010. Standard test method for measuring mass per unit area of geotextiles. American Society of Testing Materials, p. 3.
- ASTM D5199, 2012. Standard Test Method for Measuring Nominal Thickness of Geosynthetics. American Society of Testing Materials, p. 4.
- ASTM D5298, 2012. Standard Test Method for Measurement of Soil Potential (Suction) Using Filter Paper. American Society of Testing Materials, p. 6.
- ASTM D6836, 2012. Standard Test Methods for Determination of the Soil Water Characteristic Curve for Desorption Using Hanging Column, Pressure Extractor, Chilled Mirror Hygrometer, or Centrifuge. American Society of Testing Materials, p. 20.
- ASTM D4491, 2009. Standard Test Methods for Water Permeability of Geotextiles by Permittivity. American Society of Testing Materials, p. 6.
- ASTM D4716, 2014. Standard test method for determining the (in plane) flow rate per unit width and hydraulic transmissivity of a geosynthetic using a constant head. American Society for Testing Materials, p. 9.
- ASTM D7263, 2009. Standard Test Methods for Laboratory Determination of Density (Unit Weight) of Soil Specimens. American Society for Testing Materials, p. 7.
- ASTM D4318, 2010. Standard Test Methods for Liquid Limit, Plastic Limit, and Plasticity Index of Soils. American Society for Testing Materials, p. 16.
- ASTM D5856, 2015. Standard Test Method for Measurement of Hydraulic Conductivity of Porous Material Using a Rigid-Wall, Compaction-mold Permeameter. American Society for Testing Materials, p. 9.
- AFNOR G38-017, 1986. FOS from Hydrodynamic Sieving. French committee on geotextiles, p. 10.
- Benjamin, C.V., Bueno, B., Zornberg, J.G., 2007. Field monitoring evaluation of geotextile-reinforced soil retaining wall. *Geosynth. Int.* 14 (No. 2), 100–118.
- Bhattacharjee, D., Viswanadham, B.V.S., 2015. Numerical studies on the performance of hybrid-geosynthetic-reinforced soil slopes subjected to rainfall. *Geosynth. Int.* 22 (n. 6), 411–427.
- Bishop, A.W., Alpan, I., Blight, G.E., Donald, I.B., 1960. Factors controlling the strength of partly saturated cohesive soils. *Proc. Conf. Shear Strength Cohesive Soils*, ASCE 503–532, 1027–1042.
- Bouazza, A., Zornberg, J.G., McCartney, J.S., Singh, R.M., 2013. Unsaturated geotechnics applied to geoenvironmental engineering problems involving geosynthetics. *Eng. Geol.* 165 (n. 1), 143–153.
- Cabarkapa, Z., Cuccovillo, T., Gunn, M., 1999. Some aspects of the pre-failure behavior of unsaturated soil. In: *Proceedings of the 2nd International Conference on Pre-failure Behavior of Geomaterials*, Turin, vol. 1, pp. 159–165.
- Carvalho, P.A.S., Pedrosa, J.A.B.A., Wolle, C.M., 1986. Geotextile reinforced embankment – an alternative to geotechnical engineering. In: *Proceedings of Brazilian Conference on Soil Mechanics and Foundations*, 8, Porto Alegre, RS, Brazil, October 1986, pp. 169–178 (in Portuguese).
- Chamindu Deepagoda, T.K.K., Moldrup, P., Jensen, M.P., Jones, S.B., de Jonge, L.W., Schjønning, P., Scow, K., Hopmans, J.W., Rolston, D.E., Kawamoto, K., Komatsu, T., 2012. Diffusion aspects of designing porous growth media for earth and space. *Soil Sci. Soc. Am. J.* 76, 1564–1578.
- Coppola, A., 2000. Unimodal and bimodal descriptions of hydraulic properties for aggregated soils. *Soil Sci. Soc. Am. J.* 64, 1252–1262.
- Durner, W., 1994. Hydraulic conductivity estimation for soils with heterogeneous pore structure. *Water Resour. Res.* 30, 211–233.
- Ehrlich, M., Vidal, D., Carvalho, P.A., 1997. Performance of two geotextile reinforced soil slopes. In: *Proceedings of International Symposium on Recent Developments in Soil and Pavement Mechanics*, pp. 415–420. Rio de Janeiro, RJ, Brazil.
- Fredlund, D.G., Morgernstern, N.R., 1977. Stress state variables for unsaturated soils. *ASCE J. Geotech. Engng Div.* 103 (No. GT5), 447–466.
- Fredlund, D.G., Morgernstern, N.R., Widger, R.A., 1978. The shear strength of unsaturated soils. *Can. Geotechnical J.* 15 (No. 3), 313–321.
- Garcia, E.F., Gallage, C.P.K., Uchimura, T., 2007. Function of permeable geosynthetics in unsaturated embankments subjected to rainfall infiltration. *Geosynth. Int.* 14 (n. 2), 89–99.
- Chionna, V.N., Parla, P., Scotto, M., Veggi, S., 2010. Pull-out behavior of a draining geogrids embedded in waste cohesive materials. In: *Proceedings of 9th International Conference on Geosynthetics*, pp. 1319–1322. São Paulo, Brasil.
- Gourc, J.P., Matichard, Y., 1992. Development of geotextile reinforcement techniques in France – Application to retaining structures. In: *International Symposium on Geosynthetic Reinforced Soil Retaining Walls*, Netherland, pp. 131–152.
- Iryo, T., Rowe, R.K., 2005. Infiltration into an embankment reinforced by nonwoven geotextiles. *Can. Geotechnical J.* (n. 42), 1145–1159.
- Karube, D., 1988. New concept of effective stress in unsaturated soil and its proving test. *Adv. Triaxial Test. Soil Rock* 539–552. ASTM STP977.
- Kempton, G.T., Jones, C.J.F.P., Jewell, R.A., Naughton, P.J., 2000. Construction of slopes using cohesive fills and a new innovative geosynthetic material. In: *Proceedings of II European Geosynthetics Conference*, pp. 1–6. Bologna, Italia.
- Khalali, N., Khabbaz, M.H., 1998. A unique relationship for shear strength determination of unsaturated soils. *Geotechnique* 48 (No. 5), 681–688.
- Khire, M., Benson, C., Bosscher, P., 2000. Capillary barriers in semiarid and arid climates: design variables and the water balance. *J. Geotechnical Geoenvironmental Eng. ASCE* 126 (No. 8), 695–708.
- Krisdani, H., Rahardjo, H., Leong, E.C., 2010. Application of geosynthetic material in capillary barriers for slope stabilization. *Geosynth. Int.* 17 (n. 5), 323–331.
- Ling, H.I., Tatsuoka, F., Wu, J.T.H., Nishimura, J., 1993. Hydraulic conductivity of geotextiles under typical operational conditions. *Geotext. Geomembranes* 12 (n. 6), 509–542.
- McCartney, J.S., Zornberg, J.G., 2010. Effects of infiltration and evaporation on geosynthetic capillary barrier performance. *Can. Geotechnical J.* 47 (No. 11), 1201–1213. November.
- McCartney, J.S., Kuhn, J.A., Zornberg, J.G., 2005. Geosynthetic drainage layers in contact with unsaturated soils. In: *Proceedings of the Sixteenth International Conference of Soil Mechanics and Geotechnical Engineering (ISSMGE)*, Osaka, Japan, September 12–17, pp. 2301–2305.
- Mancuso, C., Vassallo, R., d'Onofrio, A., 2002. Small strain behavior of a silty sand in controlled-suction resonant column – torsional shear tests. *Can. Geotech. J.* 39 (No. 1), 22–31.
- Marinho, E.A.M., Chandler, R.J., Crilly, M.S., 1995. Stiffness measurements on an unsaturated high plasticity clay using binder elements. In: *Proc. 1st Int. Conf. On Unsaturated Soils*, vol. 2, pp. 535–539. Paris.
- Mitchell, J.K., Zornberg, J.G., 1995. Reinforced soil structures with poorly draining backfills, Part II: case histories and applications. *Geosynth. Int.* 2 (1), 265–307.
- Mualem, Y., 1976. A new model for predicting the hydraulic conductivity of unsaturated porous media. *Water Resour. Res.* 12, 513–522.
- Ng, C.W.W., Yung, S.Y., 2008. Determination of the anisotropic shear stiffness of an unsaturated decomposed soil. *Geotechnique* 58, 23–35.
- Ng, C.W.W., Xu, J., 2012. Effects of current suction ratio and recent suction history on small-strain behaviour of an unsaturated soil. *Can. Geotechnical J.* 49, 226–243.
- Perrier, H., Blivet, J.C., Khay, M., 1986. Stabilization de Talus par Renforcement tout Textile: ouvrages Experimentel et Reel. In: *Proceedings of Third International Conference on Geotextiles*, vol. 2, pp. 313–318. Vienna.
- Peters, A., Durner, W., 2008. Simplified evaporation method for determining soil hydraulic properties. *J. Hydrol.* 356 (1–2), 147–162.
- Portelinha, F.H.M., Bueno, B.S., Zornberg, J.G., 2013. Performance of nonwoven geotextile reinforced soil walls under wetting conditions: laboratory and field investigation. *Geosynth. Int.* 20 (2), 90–104.
- Portelinha, F.H.M., Zornberg, J.G., Pimentel, V., 2014. Field Performance of retaining walls reinforced with woven and nonwoven geotextiles. *Geosynth. Int.* 21 (4), 270–284.
- Schelle, H., Iden, S.C., Peters, A., Durner, W., 2010. Analysis of the agreement of soil hydraulic properties obtained from multistep-outflow and evaporation methods. *Vadose Zone J.* 9, 1080–1091.
- Stormont, J.C., Henry, K.S., Evans, T.M., 1997. Water retention function of four nonwoven polypropylene geotextiles. *Geosynth. Int.* 4 (No. 6), 572–661.
- Tan, S.A., Chew, S.H., Ng, C.C., Loh, S.L., Karunaratne, G.P., Delmas, Ph, Loke, K.H., 2001. Large-scale drainage behavior of composite geotextile and geogrid in residual soil. *Geotext. Geomembranes* 19 (3), 163–176.
- Tatsuoka, F., Yamauchi, H., 1986. A reinforcing method for steep clay slopes using a non-woven geotextile. *Geotextile Geomembranes* 4 (3), 241–268.
- Thuo, J.N., Yang, K.H., Huang, C.C., 2015. No Access Infiltration into unsaturated reinforced slopes with nonwoven geotextile drains sandwiched in sand layers. *Geosynth. Int.* 22 (n. 6), 457–474.
- Toll, D.G., 1990. A framework for unsaturated soil behavior. *Geotechnique* 40 (1), 31–44.
- van Genuchten, M.Th., 1980. A closed-form equation for predicting the hydraulic conductivity of unsaturated soils. *Soil Sci. Soc. Am. J.* 44, 892–898.
- Vanapalli, S.K., Fredlund, D.G., Pufahl, M.D., Clifton, A.W., 1996. Model for prediction of shear strength with respect to soil suction. *Can. Geotechnical J.* 33 (3), 379–392.
- Vahedifard, F., Mortezaei, K., Leshchinsky, B., Leshchinsky, D., Lu, N., 2016. Role of suction stress on service state behavior of geosynthetic-reinforced soil structures. *Transp. Geotech.* 8, 45–56.
- Wayne, M.H., Petrasic, K.W., Wilcosky, E., Rafter, T.J., 1996. An innovative use of a nonwoven geotextile in the restoration of Pennsylvania SR54. In: *Geofilters '96*, pp. 513–521. Montreal, Canada.
- Wheeler, S.J., Sivakumar, V., 1992. Development and application of a critical state model for unsaturated soils. In: *Houlsby, G.T., Schofield, A.N. (Eds.), Predictive Soil Mechanics*, pp. 709–728. T. Telford, London.
- Yamanouchi, T., Miura, N., Matsubayashi, N., Fukuda, N., 1982. Soil improvement with quicklime and filter fabric. *J. Geotechnical Eng. Div. ASCE* 108 (n. GT7), 953–965.
- Yunoki, Y., Nagao, A., 1988. An Application of non-woven fabrics to embankment of cohesive soil. In: *Proceedings of International Geotechnical Symposium on Theory and Practice of Earth Reinforcement*, pp. 491–496. Balkema, Kyushu, Japan.
- Zornberg, J.G., Arriaga, F., 2003. Strain distribution within geosynthetic-reinforced slopes. *J. Geotechnical Geoenvironmental Eng.* 129 (No. 1), 32–45.
- Zornberg, J.G., Mitchell, J.K., 1994. Reinforced soil structures with poorly draining backfills, Part I. *Geosynth. Int.* 1 (2), 103–148.
- Zornberg, J.G., Kang, Y., 2005. Pullout of geosynthetic reinforcement with in-plane drainage capability. *Geosynth. Res. Dev. Prog.* (130–142), 4135–4140. GRI-18.
- Zornberg, J.G., Bouazza, A., McCartney, J.S., 2010. Geosynthetic capillary barriers: current state of knowledge. *Geosynth. Int.* 17 (n. 5), 273–300.